

Unsteady Piston Skirts EHL at a Small and a Large Radial Clearances in the Initial Engine Start Up

Muhammad Shoaib Ansari, S. Adnan Qasim, Abdul Ghafoor, Riaz A. Mufti, M. Afzaal Malik

Abstract—In the low speed initial engine start up, the transient transverse displacements of the piston are generated in the absence of an elastohydrodynamic lubricating (EHL) film. Such transient affect the lubrication of the piston skirts and contribute towards adhesive wear. The large piston to bore radial clearance at the time of cold engine start up affects the skirts lubrication differently as compared to a hot engine re-start up at a small clearance. This study models the 2-D transient piston skirts hydrodynamic and EHL at both the large and the small radial clearances. The 2-D transient Reynolds equation is solved to generate the hydrodynamic pressures under the unsteady state conditions. The simulation results show the piston eccentricities, secondary velocities, film thicknesses and the rising pressures as the functions of 720 - degree crank rotation cycles. The outcomes suggest that the cold and hot engine start up conditions affect the hydrodynamic and EHL adversely.

Index Terms— EHL, Squeeze, Transient Modeling, Initial Engine Start up.

I. INTRODUCTION

In a few initial engine start up cycles an effective lubrication of the piston skirts has always been a challenging issue. The initial engine start up process is essentially transient in nature. Despite assuming oil flooding the engine start up wear cannot be avoided due to the initial transients and in the absence of a fully established elastohydrodynamic lubricating (EHL) film between the skirts and the cylinder liner surfaces [1]. A low initial engine start up speed allows a physical contact between the skirts and the cylinder liner that causes wear of the interacting surfaces [2]. The small secondary transients of the piston skirts have high amplitudes due to the large piston-to-bore radial clearances. Initially the size of a large radial clearance is a small fraction of a millimeter at the time of the cold engine start up. However, it gets reduced to a few microns as an engine attains normal operating conditions after a few minutes of its start up. The secondary transient displacements of the piston squeeze the

lubricant film as the skirts come closer to the liner in a few initial engine start up cycles. The squeeze action represents the unsteady time-dependent lubrication of the bearing as the lubricant flows between the interacting surfaces in relative motion [3, 4, 5]. In the initial engine start up the hydrodynamic action becomes a function of the steady wedging and an unsteady squeeze action between the piston skirts and the liner surfaces. In the hydrodynamic lubrication of the skirts an engine oil should assist in an easy cold engine start up. The viscosity of the lubricant ought to cushion the secondary eccentricities and prevent the engine start up wear. The effects of an extra space created by the large piston-to-bore radial clearance should be analyzed. It can be done by modeling the unsteady piston skirts hydrodynamic and EHL numerically at a low engine start up speed. The simulation results should be compared with those of a small radial clearance representing the normal engine operation. In the numerical models an efficient engine cooling system and isothermal conditions are assumed with 10 and 100 microns as the small and the large radial clearances, respectively. The governing equations representing the axial and transverse piston dynamics with second-order changes are solved numerically. The unsteady 2-D average Reynolds equation is discretized and solved numerically to generate the hydrodynamic pressures [5]. In the unsteady EHL model, the pressure-viscosity relationship is identified and incorporated accordingly. The elastic displacements of the interacting surfaces are incorporated to obtain the EHL film and pressure profiles. The simulation results of the hydrodynamic and EHL models at a large and a small clearance are compared to analyze their effects on the secondary eccentricities, displacement rates, film thicknesses and pressures. The following assumptions are considered in the models:

1. Newtonian lubricant with thermal effects neglected
2. Surface waviness and roughness are neglected.
3. Pressure at the inlet of contact zone is zero.
4. Flow is laminar and turbulence effects are neglected.
5. Surfaces are oil-flooded at the time of engine start up.

Table-1 (Input Parameters)

Parameter	Value	Parameter	Value
m_{pis}	0.295 kg	$\theta = \theta_1 + \theta_2$	75 degree
R	0.0415 m	l	0.133 m
L	0.0338 m	η	0.08571 Pa.S.
m_{pin}	0.09 kg	v_1, v_2	0.3
R	0.0418 m	E_1, E_2	200 GPa

This work was sponsored by National University of Sciences and Technology (NUST), Islamabad, Pakistan. Financial support was provided by the Higher Education Commission of Pakistan.

Muhammad Shoaib Ansari is research assistant at NUST School of Mechanical and Manufacturing Engg. (email: shoibansari15@yahoo.com)

Syed Adnan Qasim is research associate at NUST College of Electrical and Mechanical Engineering. (email: adnan_qasim@yahoo.com)

Abdul Ghafoor is Professor and Dean at NUST School of Mechanical and Manufacturing Engineering (email: aghafoor@smme.nust.edu.pk)

Riaz A. Mufti is Associate Professor at NUST School of Mechanical and Manufacturing Engineering (email: dr.mufti@hotmail.com)

M. Afzaal Malik is Professor at Department of Mechanical and Aerospace Engg. Air University. (email: drafzaalmalik@yahoo.com)

II. MATHEMATICAL MODEL

A. Governing Equations of Piston Motion

The mathematical relationships dealing with the piston dynamics are defined. The secondary eccentricities or displacements of the piston along the direction perpendicular to the axis of cylinder are defined. For constant crankshaft speed ω , the piston speed is [6]:

$$U = \dot{Y} = r\omega \sin \Psi + r\omega B \cos \Psi (l^2 - B^2)^{-0.5} \quad (1)$$

$$\text{where } B = C_p + r \sin \Psi \quad (2)$$

The second-order time-dependent displacements of the top and the bottom sides of the piston skirts are calculated. The inertia of the piston, forces and moments in equilibrium are incorporated in the form suggested by Zhu et al [7]:

$$\begin{bmatrix} a_{11} & a_{12} \\ a_{21} & a_{22} \end{bmatrix} \begin{bmatrix} \ddot{e}_t \\ \ddot{e}_b \end{bmatrix} = \begin{bmatrix} F + F_s + F_f \tan \phi \\ M + M_s + M_f \end{bmatrix} \quad (3)$$

$$a_{11} = m_{pis} \left(1 - \frac{a}{L}\right) + m_{pis} \left(1 - \frac{b}{L}\right) \quad (3a)$$

$$a_{12} = m_{pis} \frac{a}{L} + m_{pis} \frac{b}{L} \quad (3b)$$

$$a_{21} = \frac{I_{pis}}{L} + m_{pis} (a - b) \left(1 - \frac{b}{L}\right) \quad (3c)$$

$$a_{22} = m_{pis} (a - b) \frac{b}{L} - \frac{I_{pis}}{L} \quad (3d)$$

B. Reynolds Equation and Hydrodynamic Pressure

The 2-D unsteady Reynolds equation is solved numerically after incorporating the time-dependent squeeze effects. The unsteady Reynolds equation in dimensional form is [6]:

$$\frac{\partial}{\partial x} \left(h^3 \frac{\partial p}{\partial x} \right) + \frac{\partial}{\partial y} \left(h^3 \frac{\partial p}{\partial y} \right) = 6\eta U \frac{\partial h}{\partial y} + \frac{\partial h}{\partial t} \quad (4)$$

The non-dimensional unsteady Reynolds equation is [6, 8]:

$$\frac{\partial}{\partial x^*} \left(h^{*3} \frac{\partial p^*}{\partial x^*} \right) + \left(\frac{R}{L} \right)^2 \frac{\partial}{\partial y^*} \left(h^{*3} \frac{\partial p^*}{\partial y^*} \right) = \frac{\partial h^*}{\partial y^*} + \frac{\partial h^*}{\partial t^*} \quad (5)$$

Boundary conditions for Reynolds equation are [6, 7]:

$$\begin{aligned} \frac{\partial p}{\partial x_{x=0}} &= \frac{\partial p}{\partial x_{x=\pi}} = 0 ; \\ p &= 0 \text{ when } x_1 \leq x \leq x_2 \\ p(x, 0) &= p(x, L) = \end{aligned} \quad (6)$$

C. Hydrodynamic Forces and Shear Stress

The hydrodynamic and the friction forces are [7]:

$$F_h = R \iint p(x, y) \cos x \, dx dy \quad (7)$$

$$F_{fh} = R \iint \tau(x, y) \, dx dy \quad (8)$$

$$F_{fh} = \iint \left(\eta \frac{U}{h} + \frac{h}{2} \frac{dp}{dy} \right) \, dx dy \quad (9)$$

The total normal force acting on the piston skirts is [6, 7]:

$$F_s = \tan \phi (F_G + F_{IP} + F_{IC}) \quad (10)$$

D. Film Thickness in Hydrodynamic Regime

By considering the time-dependent piston eccentricities, the film thickness of the lubricant is [7]:

$$h = C + e_t(t) \cos x + [e_b(t) - e_t(t)] \frac{y}{L} \cos x \quad (11)$$

E. Film Thickness in EHL Regime

In the EHL regime the bulk elastic displacement is considered. The EHL film thickness is [7, 9]:

$$h_{ehI} = h + f(\theta, y) + v \quad (12)$$

where $f(\theta, y)$ defines the profile due to manufacturing imperfections and is neglected. The differential surface displacement is [7, 9]:

$$dU = \frac{1}{\pi E'} \frac{p(x, y) dy dy}{\dot{r}} \quad (13)$$

$$\text{where } \dot{r} = \sqrt{(x - x_0)^2 + (y - y_0)^2} \quad (14)$$

$$\frac{1}{E'} = \frac{1}{2} \left[\frac{(1 - \nu_1^2)}{E_1} + \frac{(1 - \nu_2^2)}{E_2} \right] \quad (15)$$

The elastic displacement at a specific point (x_0, y_0) is [9]:

$$U(x_0, y_0) = \frac{1}{\pi E'} \iint_A \frac{p(x, y) dx dy}{\dot{r}} \quad (16)$$

III. NUMERICAL RESULTS AND DISCUSSION

Equation (3) defines the secondary piston dynamics in the state-space algebraic form. The numerical solution of a pair of non-linear equations, which constitutes an initial value problem provides the time-based secondary eccentricities of the piston. The values of e_p , e_b , \dot{e}_t and \dot{e}_b are guessed at a previous time step, which become the initial values for the current time step to solve equation (12). It gives the hydrodynamic film thickness at the current time step. An appropriate size finite difference mesh is generated and the time marching is carried out at an appropriate time step by using the forward time central space (FTCS) scheme. The initial time step size is adjusted continuously to arrive at a converged solution based on the pre-defined convergence criteria. The convergence of the solution provides the hydrodynamic pressures based on the unsteady Reynolds equation and the oil film thickness equation. Then we calculate all the forces and moments in equation (4) and compute the accelerations \ddot{e}_t , \ddot{e}_b to satisfy from the solution of velocities \dot{e}_t , \dot{e}_b at previous and present time steps. When secondary velocities \dot{e}_t , \dot{e}_b are satisfied, the piston position at the end of the current time step is determined as [7]:

$$\begin{aligned} e_t(t_i + \Delta t) &= e_t(t_i) + \Delta t \dot{e}_t(t_i) \\ e_b(t_i + \Delta t) &= e_b(t_i) + \Delta t \dot{e}_b(t_i) \end{aligned}$$

A 4-stroke cycle of an engine implies two 360 degree crankshaft revolutions. It means that $4\pi = 720$ degrees crank angle. The convergence criteria of the periodic solution is defined based on 4π . The solution should satisfy [7]:

$$\begin{aligned} e_t(t) &= e_t \left(t + \frac{4\pi}{\omega} \right); & e_b(t) &= e_b \left(t + \frac{4\pi}{\omega} \right) \\ \dot{e}_t(t) &= \dot{e}_t \left(t + \frac{4\pi}{\omega} \right); & \dot{e}_b(t) &= \dot{e}_b \left(t + \frac{4\pi}{\omega} \right) \end{aligned}$$

A. Piston Eccentricities and Velocities

Figures 1 and 2 shows the dimensionless eccentric displacement profiles of the top and the bottom surface of the piston skirts in the hydrodynamic and EHL regimes, respectively. The E_t and the E_b curves in each sub-figure show the respective piston eccentricities at a small and a large radial clearance. Each figure shows the three horizontal lines such that the top, middle and the bottom lines are at $+1$, 0 and -1 , respectively. The top and the bottom lines represent the liner walls on the non-thrust and the thrust sides, respectively. The middle line indicates that concentricity exists between the piston and the liner axes. If the E_t or the E_b curve touches either the top or the bottom line then a physical contact between the skirts and the liner will get established and wear will take place. The profile curves are plotted against the 720 degree 4-stroke cycle on the horizontal axis. The induction, compression, expansion and exhaust strokes are represented by 0-180, 181-360, 361-540 and 541-720 degrees of crank angle, respectively. For a constant crank speed the piston translates between the top dead centre (TDC) and the bottom dead centre (BDC) at the cyclic speed. At 10 microns clearance, the piston starts sliding concentrically. It achieves a maximum cyclic speed at the mid- induction stroke before getting displaced eccentrically towards the non-thrust side. At the end of the induction stroke at BDC, the sliding direction of the piston changes and it compresses the inducted air-fuel charge in the compression stroke. The directional shift increases the film thickness of the lubricant and displaces the skirts eccentrically further towards the top line. In the compression stroke, the intake and the exhaust valves are closed. The piston compresses the air-fuel mixture, which increases the amplitude of the gas pressure force, significantly. The buildup of the hydrodynamic pressures intensifies with steeper gradients and the film gets thicker. The eccentrically placed piston skirts shift towards the middle line. The instantaneous piston concentricity is achieved before the piston goes past the middle line. A fully compressed air-fuel mixture and a very high magnitude of the gas force at the end of the compression stroke do not let the piston to eccentrically displace substantially. Combustion occurs in the beginning of the expansion stroke. It produces a substantial thrust to displace the piston and the top surface goes very close to the bottom line. The impetus of the combustion thrust subsides after the piston goes past the mid-expansion stroke. The exhaust valves open before the end of the expansion stroke. The hydrodynamic pressures drop and the effect of the gas force subsides significantly. The absence of any external force does not let the skirts to displace further till the end of the exhaust stroke. At the radial clearance of 10 microns there is no physical contact between the skirts and the liner surfaces in the hydrodynamic lubrication regime. However the extensive loading enhances the hydrodynamic pressures. Under the combined squeeze and wedging action the pressures deform the interacting surfaces elastically in the EHL regime. The loading fails to prevent a solid-to-solid contact between the surfaces. At 100 microns clearance the physical contact at the thrust side cannot be avoided in the hydrodynamic and EHL regimes. Figures 3 and 4 show the profiles of the secondary velocities of the top and the bottom surfaces of the skirts, represented as $E_{t\dot{}}$ and $E_{b\dot{}}$, respectively. The velocity profiles are shown in the positive and the negative quadrants, respectively. The profiles in positive quadrant imply that the energy transfer

takes place from the skirts to the liner surface. Those in the negative quadrant mean the transfer of energy from the liner to the skirts surface. A comparison of the respective profiles at 10 and 100 microns clearance shows that the amplitudes of the velocity curves affect the secondary eccentricities. In the hydrodynamic regime the amplitudes are visibly smaller in the negative quadrant at 10 microns than those at 100 microns. Resultantly, the physical contact between the skirts and the liner is avoided conveniently. In the EHL regime the almost same amplitudes imply a physical contact between the opposing surfaces and wear.

B. Hydrodynamic Pressures

The 3-D buildup of the hydrodynamic pressures over the surface of the skirts at some of the significant piston positions are shown in figures 5 and 6. In both the radial clearance cases the positive pressures are biased towards the top surface during the entire duration of the 720 degree crank rotation cycle. This trend is in contrast with the case of a steady hydrodynamic lubrication when the bias of pressures shifts towards the bottom surface in the expansion stroke [1]. At 10 microns clearance the low pressures buildup gradually with gentle slopes at the mid-induction stroke. At the end of the compression stroke the high peak pressures shift to the right and the intense pressures rise swiftly with steep gradients. Under the influence of the time-dependent squeeze effect the parabolic shape of the pressure fields is transformed into the sharply rising pressures with pointed peaks in the expansion and the exhaust strokes. A comparison of the hydrodynamic pressure fields at the stated clearances shows that the squeeze effects are more pronounced at 10 microns than at 100 microns. In both the cases the slopes of the rising pressures are gentle during the induction stroke. However the pressure intensities and the gradients start changing during the compression stroke. At the end of the compression stroke the gradients vary such that the slopes are steeper at 10 microns clearance. The squeeze effects are visibly pronounced after combustion and the magnitudes of the rising pressures are higher at 10 microns than at 100 microns clearance. The steeper slopes represent the higher intensities of the pressures that buildup during the expansion and the exhaust strokes at 10 microns clearance. It shows that by reducing the piston-to-bore radial clearance the hydrodynamic pressures intensify and buildup sharply.

C. Film Thickness in Hydrodynamic and EHL Regimes

Figures 7(a) and 8(a) show the maximum and the minimum hydrodynamic film thickness profiles at the stated clearances. Apart from this, the film thickness profiles in the EHL regime at the maximum hydrodynamic pressures prior to the elastic deformation and after the displacements are also shown. The *EHL Film* profile is separately shown also in figures 7(b) and 8(b), respectively. In the hydrodynamic lubrication regime, the maximum and minimum film thickness profiles are represented as the *Max. Hyd. Film* and *Min. Hyd. Film*, respectively. In the hydrodynamic regime, the thickness of the maximum film represents the profile prior to the application of the load whereas, the minimum film actually carries the hydrodynamic load. The hydrodynamic film thickness profiles are generally similar in both the stated cases but the magnitudes vary significantly. The general similarity in the respective profiles is attributed

to the dominating effect of squeeze action as a function of time as compared to the steady state side leakage effect due to the wedging action. Despite a large radial clearance at 100 microns the minimum film thickness does not rise significantly under the effect of dynamic squeeze loads. The hydrodynamic films get thicker with each eccentric piston displacement in the induction and the compression strokes in both the cases. In the compression stroke combustion reduces the film thicknesses drastically. In the EHL regime the combined wedging and squeeze effects increase the loading. The loads increase and deform the surfaces after attaining the maximum values. Under the oil flooding conditions the additional space created due to the elastic surface displacements is readily occupied by the lubricant, which increases the EHL film thickness. At 10 microns radial clearance the EHL film does not rise substantially. However, it is not the case when the clearance is 100 microns. It implies that despite the combined hydrodynamic and squeeze effects a large radial clearance does not permit a substantial reduction in the hydrodynamic film thickness. It implies that if there are insufficient pressures in the EHL regime then the loading will not permit the glass-like transition of the EHL film and the lubricant will remain in the rigid hydrodynamic regime. The liquid lubricant film in the rigid hydrodynamic regime may rupture with the application of a sudden instantaneous load. The film rupture may cause excessive wear when the surfaces are subjected to fairly high loads in the hydrodynamic regime.

D. Pressure Rise in EHL Regime

The pressures buildup in the hydrodynamic lubrication regime is gradual under the application of low loads of varying intensities. Under the influence of the time dependent normal loads and the hydrodynamic action due to the tangential loading they are biased towards the top surface of the skirts for the entire duration of the 720 degrees crank rotation cycle. The very small and large radial clearances impact the magnitudes of the generated pressures. In the EHL regime the pressures intensify to very high proportions and actually deform the surfaces. The extent of deformation depends upon the magnitudes of the high intensity pressures. The magnitudes are influenced by the piston-to-bore radial clearance such that a very large clearance does not allow sufficient a sufficient rise in the pressures to deform the surfaces appreciably. Resultantly, either the film thickness remains in the hydrodynamic regime or it fails to cause sufficient elastic displacements to enhance the film thickness. Figure 9 shows the maximum rise of the generated pressures, which causes the elastic surface displacements in the EHL regime. At 10 microns radial clearance the pressures rise more than in the case of 100 microns. It implies that the large radial clearance affects the amplitudes of the rising pressures. Moreover, the bias of the maximum pressures shifts from the center of the skirts surface to the mid-point of the bottom side at 100 microns radial clearance. The low intensity pressures rising over the bottom shift their bias from the bottom side to near the top surface of the skirts when the piston-to-bore radial clearance is increased from a small value to a fairly large one.

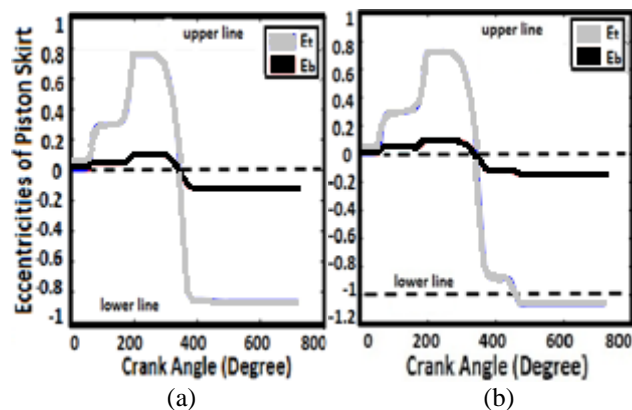


Fig:1 Dimensionless Piston Skirts Eccentricities in Hydrodynamic Regime at (a) 10 microns (b) 100 microns

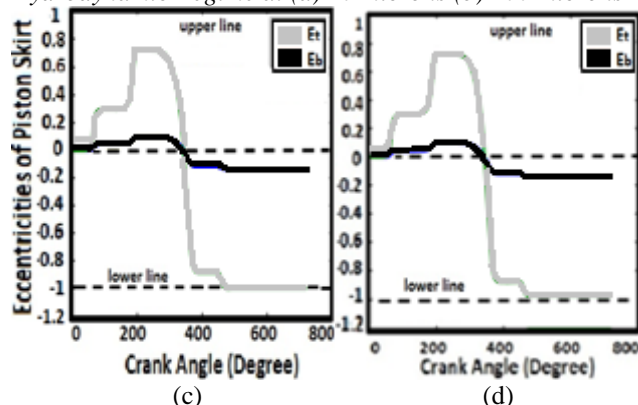


Fig:2 Dimensionless Piston Skirts Eccentricities in EHL Regime at (a) 10 microns (b) 100 microns

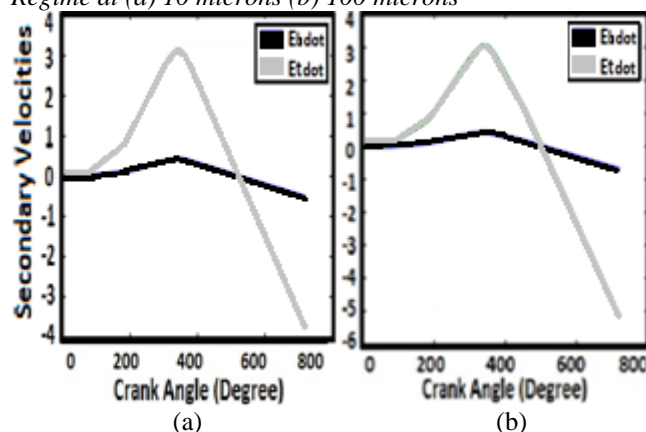


Fig:3 Dimensionless Skirts Eccentric Displacement Rates in Hydrodynamic Regime at (a) 10 microns (b) 100 microns

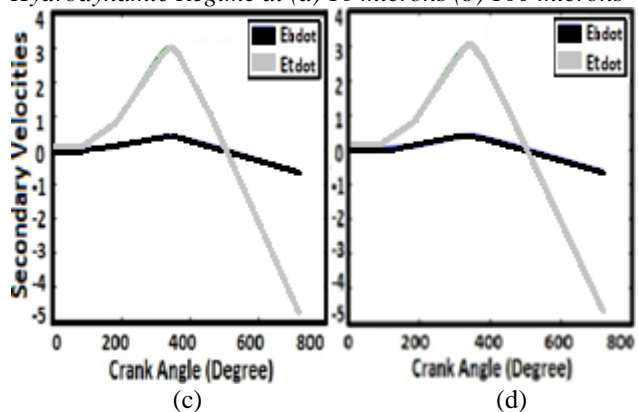
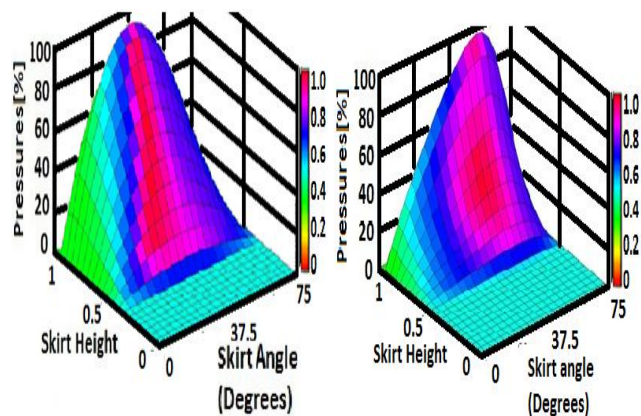
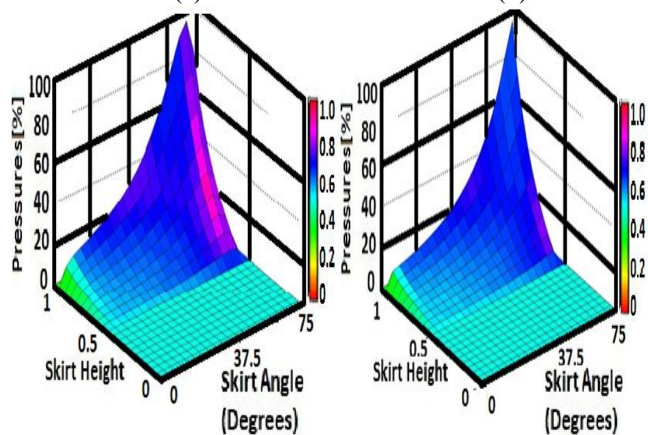


Fig:4 Dimensionless Piston Skirts Eccentric Displacement Rates in EHL Regime at (a) 10 microns (b) 100 microns

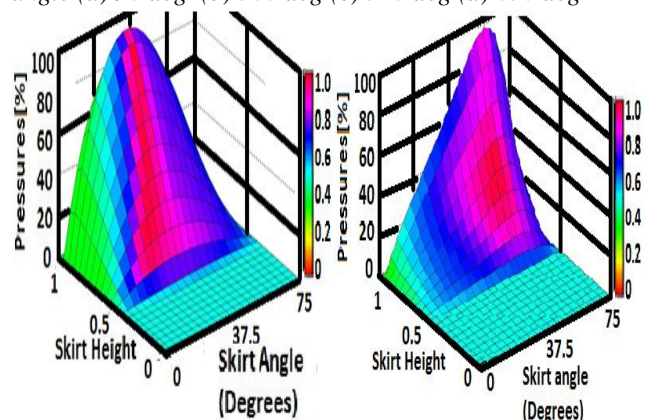


(a) (b)

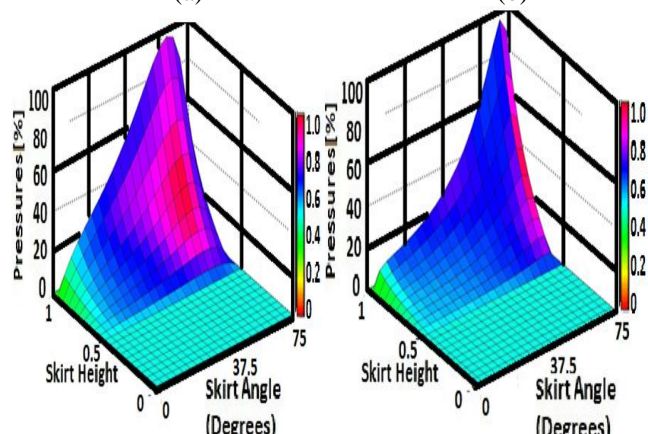


(c) (d)

Fig:5 Hydrodynamic Pressure Fields at 10 microns at crank angle (a) 90 deg (b) 360 deg (c) 540 deg (d) 630 deg

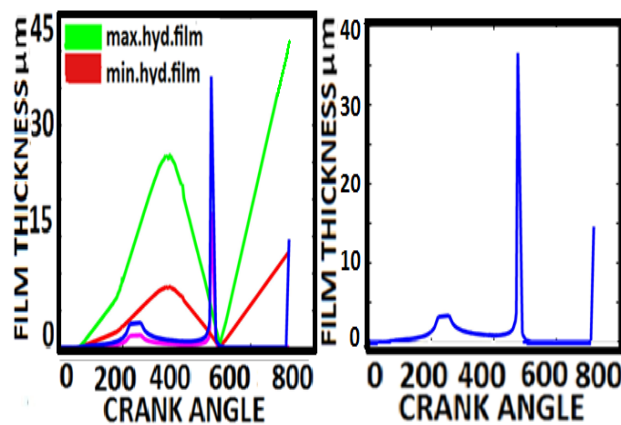


(a) (b)



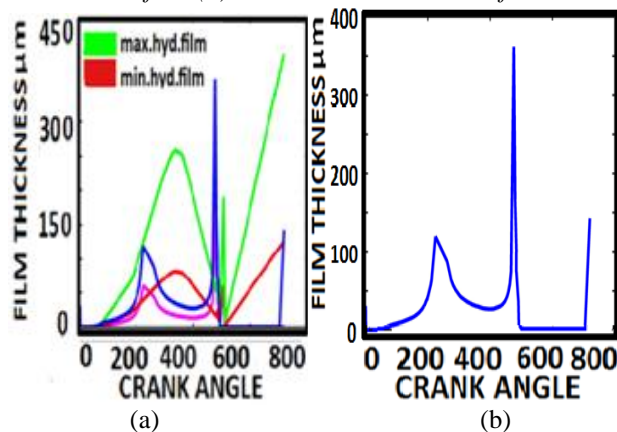
(c) (d)

Fig:6 Hydrodynamic Pressure Fields at 100 microns at crank angle (a) 90 deg (b) 360 deg (c) 540 deg (d) 630 deg



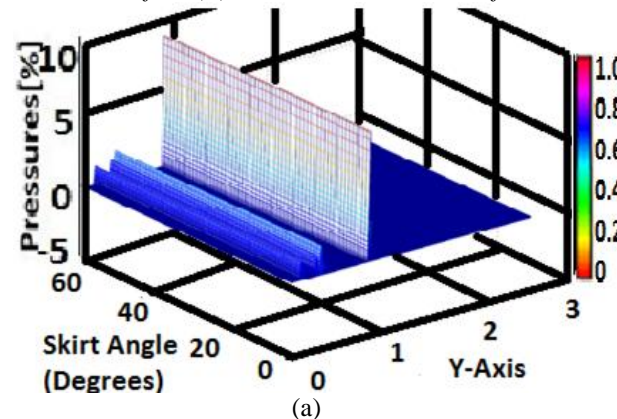
(a) (b)

Fig: 7 At 10 microns Clearance (a) Hydrodynamic Film Thickness Profiles (b) EHL Film Thickness Profile

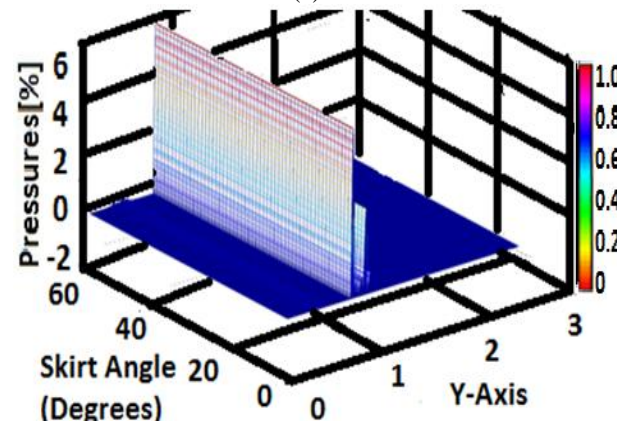


(a) (b)

Fig: 8 At 100 microns Clearance (a) Hydrodynamic Film Thickness Profiles (b) EHL Film Thickness Profile



(a)



(b)

Fig: 9 Dimensionless EHL Pressure Rise at (a) 10 microns (b) 100 microns

IV. CONCLUSIONS

In this paper, we have studied the effects of a very small and a substantially large piston-to-bore radial clearance on the unsteady hydrodynamic and EHL of piston skirts. The unsteady modeling involves the transients which depend on the time-dependent squeeze effects. Fairly viscous Newtonian engine oil was used to model the lubrication of piston skirt surface in a few unsteady initial engine start up cycles. The simulation results of the numerical models reveal that the time-dependent squeeze effects influence the hydrodynamic pressure generation. The large radial clearances affect the formation of the EHL film, which is essential to prevent the engine start up wear. When the squeeze term is introduced in the piston skirts lubrication model then a large radial clearance cannot prevent the engine start up wear. However, it may be prevented in the rigid hydrodynamic regime if a very small clearance is considered at the time of the initial engine start up. In case of a small clearance the hydrodynamic pressures rise fairly high as compared to the case of a large radial clearance. In case of lubricant starvation the engine start up wear increases. At a large radial clearance the pressures do not rise to higher values to deform the interacting surfaces and improve the EHL film thickness. It leaves behind the possibility of low load-carrying capacity of the lubricant. Hence, the large radial clearance may be avoided if the unsteady squeeze effects are more pronounced at the time of the application of the load. In view of the findings the small radial clearance may be preferred over the large radial clearance under the stated conditions. However, further studies are needed at the other piston-to-bore radial clearances by using the low and the high-viscosity grade engine lubricants.

Nomenclature

C = Piston radial clearance
 C_f = Specific heat of lubricant
 C_g = Distance from piston center of mass to piston pin
 C_p = Distance of piston-pin from axis of piston
 E_1, E_2 = Young's Modulus of piston and liner
 F = Normal force acting on piston skirts
 F_f = Friction force acting on skirts surface
 F_{fh} = Friction force due to hydrodynamic lubricant film
 F_G = Combustion gas force acting on the top of piston
 F_h = Normal force due to hydrodynamic pressure in the film
 F_{IC} = Transverse Inertia force due to piston mass
 $\overline{F_{IC}}$ = Reciprocating Inertia force due to piston mass
 F_{IP} = Transverse Inertia force due to piston-pin mass
 $\overline{F_{IP}}$ = Reciprocating Inertia force due to piston-pin mass
 I_{pis} = Piston rotary inertia about its center of mass
 L = Piston skirt length
 M = Moment about piston-pin due to normal forces
 M_f = Moment about piston-pin due to friction force
 M_{fh} = Moment about piston pin due to hydrodynamic friction
 M_h = Moment about piston pin due to hydrodynamic pressure
 R = radius of piston
 U = Piston Velocity
 a = Vertical distance from piston skirt top to piston pin
 b = Vertical distance from piston skirt top to center of gravity
 \ddot{e}_b = Acceleration term of piston skirts bottom eccentricities

\ddot{e}_t = Acceleration term of piston skirts top eccentricities
 l = Connecting rod length
 m_{pis} = Mass of piston
 m_{pin} = Mass of piston pin
 p = Hydrodynamic pressure
 r = Crank radius
 \dot{r} = Radius of piston
 u = Lubricant velocity component along x direction
 v = Lubricant velocity component along y direction
 τ = Shear stress
 ψ = Crank angle
 η = Viscosity at ambient conditions
 Φ = Connecting rod angle
 ω = Crank rotation speed
 U_1, U_2 = Poisson's ratio
 ν = Elastic deformation of piston skirts
 θ = Piston skirts angle in degree

REFERENCES

- [1] M Afzaal Malik, S. Adnan Qasim, Badar R., S. Khushnood, "Modeling and Simulation of EHL of Piston Skirts Considering Elastic Deformation in the Initial Engine Start up," Proc. 2004 ASME/STLE Int. Joint Tribol. Conf. Trib2004-64101
- [2] S. Adnan Qasim, M. A. Malik, M. A. Khan, R. A. Mufti, 2011, "Low Viscosity Shear Heating in Piston Skirts EHL in Low Initial Engine Start up Speeds", *Tribol. International*, Vol.44(10), pp. 1134-43.
- [3] Roberto F. Ausas, Mohammed Jai and Gustavo C. Buscaglia, "A mass-conserving algorithm for dynamical lubrication problems with cavitation", ASME Journal of Tribology, July 2009, Vol. 131 / 031702-7.
- [4] Ilya I. Kudish, Rubber G. Airapetyan and Michael J. Covitch, "Modeling of Lubricant Degradation And EHL," IUTAM Symposium on EHD and Micro EHDs, 1st ed. 149-1, 2006, Springer.
- [5] Optasanu, V. and Bonneau, D., "Finite element mass-conserving cavitation algorithm, 2000, Transactions of the ASME.
- [6] Dong Zhu, Herbert S. Cheng, Takayuki Arai, Kgugo Hamai, "A Numerical Analysis for Piston Skirts in Mixed Lubrication," ASME. 91-Trib-66.
- [7] S. Adnan Qasim, M. Afzaal Malik, Mumtaz Ali Khan, Riaz A. Mufti, March 2012, "Modeling Shear Heating in Piston Skirts EHL Considering Different Viscosity Oils in Initial Engine Start Up", ASME J. Eng. for Gas Turbines and Power, Vol. 134, Issue 3, pp. 032802-10
- [8] Gwidon W. Stachowiak and Andrew W. Batchelor, (Book) *Engineering Tribol*, 3rd Ed., Elsevier; pp. 112-219 I
- [9] Dowson D., Higginson G.R., Book, "Elasto-Hydrodynamic Lubrication: The Fundamentals of Gear And Roller Lubrication", 1966, pp 55-106.